Fluorinated *vs.* Non-fluorinated PR_2(biaryl) Ligands and their [AuCl(L)] Complexes: Synthesis, X-ray Structures, and Computational Study of Weak Interactions. Bond, no Bond, and Beyond

Jaime Ponce-de-León, Rebeca Infante, María Pérez-Iglesias, and Pablo Espinet*

[a] IU CINQUIMA/Química Inorgánica, Facultad de Ciencias, Universidad de Valladolid, 47071 Valladolid (Spain).

KEYWORDS (Word Style "BG_Keywords"). If you are submitting your paper to a journal that requires keywords, provide significant keywords to aid the reader in literature retrieval.

Supporting Information Placeholder

ABSTRACT: Six fluorinated PR_2(biaryl) phosphines, L^n, with R = Ph, Cy and biaryl = C_6H_4-C_6F_5, C_6F_4-C_6H_5, or C_6F_4-C_6F_5, have been prepared. Their [AuCl(L^n)] complexes and H congeners with PhJohnPhos or CyJohnPhos have been studied in order to examine the interactions that bring the distal aryl close to the Au–Cl bond region. X-ray, DFT structure optimization, QTAIM, and NCI methods allow for some understanding of the forces involved. The "no bond" non-covalent distal-aryl/Au–Cl weak interactions are produced at forced short distances achieved under intramolecular structural ligand pressure. Enhanced vdW distal-aryl/Au interactions at "no bond" distances shorter than the sum of Au and C vdW radii, and weaker distal-aryl/Cl interactions at "no bond" distances beyond the sum of Cl and C vdW radii, counterbalance the unfavorable structural distortion of the free ligand, providing some extra stability of the molecule in the order 2-10 kcalmol^{-1}. The F substituents in the distal aryl induce shorter aryl distances to the Au–Cl zone, pointing overall to stronger π-aryl polarization as the main responsible of NCIs with gold. The interactions in the C···Cl zone, where the distances are larger than the sum of vdW radii, contribute only about 5%, according to energy estimations using NBOs.

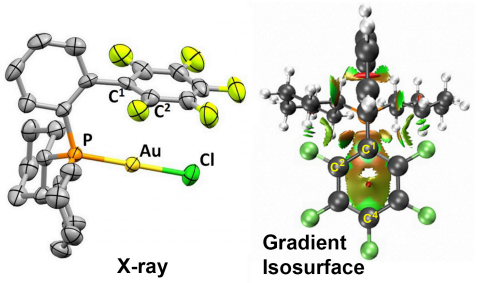

INTRODUCTION

PR_2(biaryl) ligands have revolutionized the C–C and C–N Pd catalytic coupling processes, in which they are particularly powerful. Along their development, these ligands have been modified with incorporation of different groups (often alkoxy groups) in the biaryl moiety, usually aimed at protecting the ligands from undesired reactions or at improving their catalytic performance.[1] In most of these phosphines the distal aryl of the biaryl group is either phenyl or an electron-enriched aryl. Only in a few reported cases the biaryl fragment is partially fluorinated in the distal aryl (Figure 1).[2]

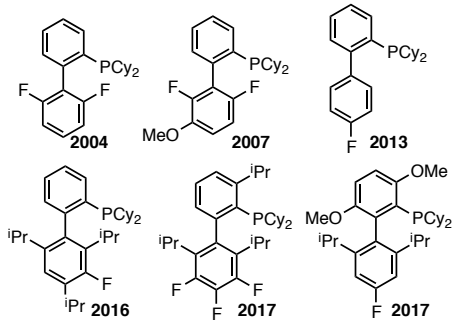

Figure 1. Reported Buchwald-type partially fluorinated biaryl phosphines.

Biaryl phosphines have been also frequently used in gold(I) catalysis,[3] often in cyclization or cycloaddition reactions catalyzed by cationic complexes. In the X-ray diffraction structures of [AuX{PR_2(biaryl)}] complexes, whether cationic or neutral, the distal aryl of the biaryl group is systematically located roughly parallel to the Au–X bond, with one or two aryl carbon atoms at distances from gold in the range 3.02-3.30 Å. These structures have been examined in several occasions.[4] The proximity of the distal aryl to gold suggests mutual interactions, often referred to as *weak interactions*, sometimes as *π-interactions*. Recently, two theoretical studies on [AuX{PR_2(biaryl)}] complexes have been published: one on the R_F effect in a family of [Au(SR_F)(JPhos)] thiolate complexes, JPhos = P(*t*-Bu)$_2$(C_6H_4-C_6H_5);[5] and another, on Tolman cone angles of P-ligands in different metal coordinations, including [AuCl(PR_2(biphenyl)] examples.[6]

Here we report the synthesis of six new biaryl phosphines fully fluorinated either at the proximal aryl (relative to P), at the distal aryl, or at both aryls (Figure 2), and their corresponding [AuCl{PR_2(biaryl)}] (R = Ph, Cy) complexes. Including in the further study the reported non-fluorinated PhJohnPhos (**PhJ**) and CyJohnPhos (**CyJ**) phosphines, we complete, for R = Ph, Cy, the

sequences HH, HF, FH, and FF relative to proximal and distal aryl-perfluorination or non-fluorination. These two series (eight complexes) provide us with a privileged position to study the interactions with the Au–Cl zone of electronically different distal-aryls.

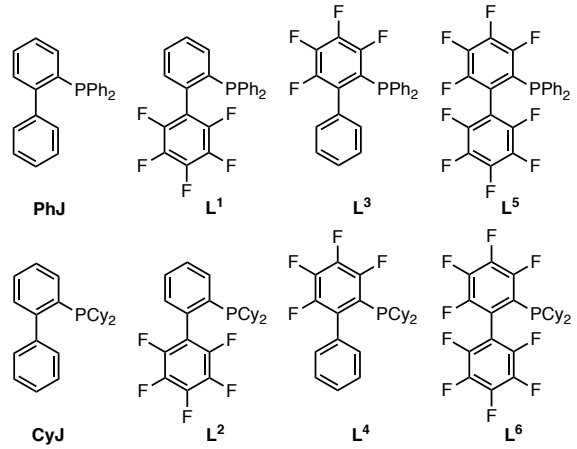

Figure 2. Fluorinated Buchwald-type biaryl phosphines reported and used in this work, and their two reference non-fluorinated phosphines.

RESULTS AND DISCUSSION

Synthesis of the ligands and their gold(I) complexes.

The new ligands L^1-L^6 were obtained by lithiation of the corresponding biaryl bromide with Li(*n*-Bu) followed by reaction with PR_2Cl (R = Ph, Cy), as sketched in Scheme 1.[7] The addition of the **L^n** ligand to [AuCl(tht)] (tht = tetrahydrothiophene) affords colorless [AuCl(L^n)] (**1**-**6**) complexes, labeled according to the **n** number in the ligand. The reported **PhJ** and **CyJ** ligands provide non-fluorinated H-homologues for comparison.[4b,8]

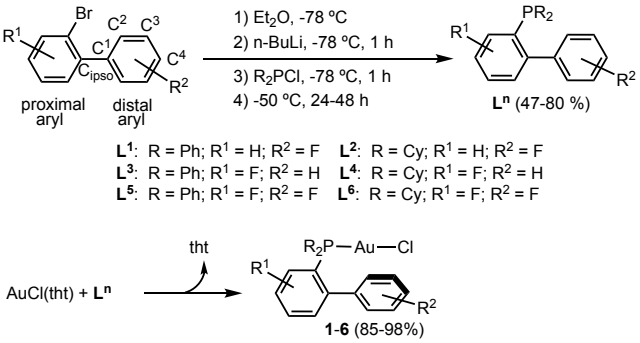

Scheme 1. Synthesis of fluorinated biaryl phosphines and their gold (I) complexes. R = Ph or Cy; R^1, R^2, or both are all F. The number of the complex is as the superindex of its **L^n** ligand.

Experimental and calculated structures. Structural analysis.

Colorless needles were obtained for the six new gold complexes by slow diffusion of a CH_2Cl_2 solution of the complex in *n*-hexane. Their X-ray structures are shown in Figure 3. The crystal of **6** contains two non-equivalent molecules, **6a** (shown in Figure 3) and **6b** (shown in Fig. S1), with only slightly different molecular parameters. Both converge to the same DFT structure in the gas phase (see later). There is, in the whole **1-6** series, just a short range of variation of Cl–Au–P angles (176.5-179.4), and Au–Cl (2.271-2.290 Å) or Au–P (2.226–2.238 Å) distances (Table S1, experimental), excepting **6b**, which is a bit out of these ranges. As expected, all the X-ray diffraction structures display almost linear Cl–Au–P coordination, with the distal aryl group lying close to parallel to the Au–Cl bond. Being more precise, the distal aryl ring bends away from the Au–Cl bond so that C^1 has a noticeably shorter distance to this line than C^4. Typical reported bending angles between the Au–P and the C_{ipso}–C^1 inter-ring vectors are in the range 15-20°.[4c] This distortion, although small, suggests that these are not the structures that these molecules should adopt in the absence of other forces compensating this angular distortion. This is discussed later.

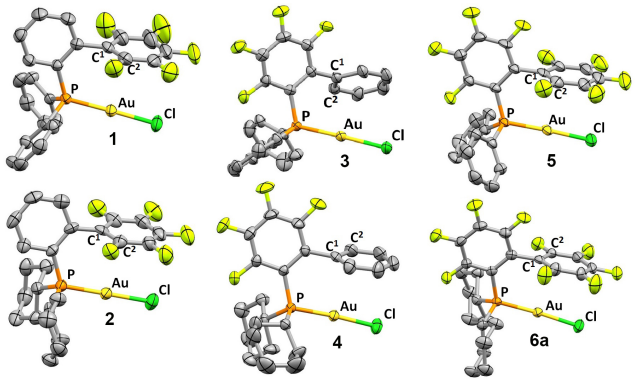

Figure 3. X-ray diffraction structures of complexes [AuClL^n] **1**–**6**. H atoms omitted for clarity.

Table 1 (see Scheme 1 for labelling) collects in columns 2 and 3 the Au–C distances of the two distal-aryl carbon atoms closer to Au, for **1-6** and their non-fluorinated congeners [AuCl(**PhJ**)] and [AuCl(**CyJ**)] (the two latter taken from the literature).[4b,8] The shortest distances for each complex is Au–C^1, always shorter than the sum of Bondi vdW radii (3.36 Å).[9] Noticeably shorter than the rest are the distances found in two fluorinated complexes (**4** and **5**). Beyond that, a clear case-by-case analysis of structure/Au–C distance relationship is not obvious.

Table 1. Experimental Au-C and Au–Cl distances (Å) in the X-ray diffraction [AuCl(L^n)] structures. PhHF indicates the ligand with Ph_2P, H in the proximal aryl and F in the distal aryl, and similarly for the others.

Complex	Au-C^1	Au-C^2	Cl-C^3	Cl-C^4
AuCl(**PhJ**) (PhHH)	3.235	3.402	4.082	3.968
AuCl**L^1** (PhHF) (**1**)	3.179	3.259	3.681	3.591
AuCl**L^3** (PhFH) (**3**)	3.149	3.390	3.986	4.235
AuCl**L^5** (PhFF) (**5**)	3.097	3.313	3.589	3.418
AuCl(**CyJ**) (CyHH)	3.151	3.298	4.082	3.968
AuCl**L^2** (CyHF) (**2**)	3.159	3.188	3.574	3.431
AuCl**L^4** (CyFH) (**4**)	3.066	3.235	3.598	3.727
AuCl**L^6** (CyFF) (**6a**)	3.141	3.178	3.608	3.450
(**6b**)	3.171	3.303	3.986	3.602

Two structurally different kinds of X-ray structures are observed as shown in the two examples above in Figure 4. Most of them (**1**, **5**, AuCl(**CyJ**), **2**, **6A**, and **6B**), are quite symmetrical, with the Au–Cl line almost exactly over the C^1–C^4 line. In the others (AuCl(**PhJ**), **3**, **4**), these two lines deviate.

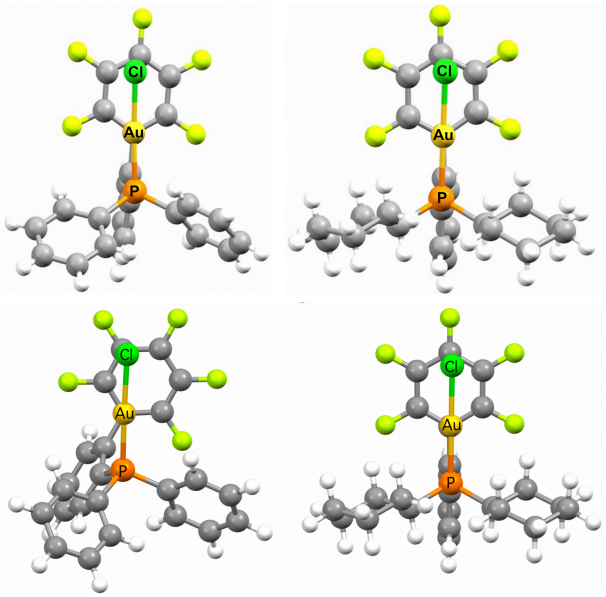

Figure 4. Examples of X-ray (the two above) and gas phase DFT calculated (the two below) structures of [AuCl**L**^{1}] (left) and [AuCl**L**^{2}] (right), viewed along the Au···C^1 imaginary line (in this view, C^1 is eclipsed by the Au above it).

In order to compare structures not altered by crystal forces, DFT calculations were carried out to obtain optimized gas phase molecular structures (*e.g.* the two in Figure 4, below). First, calculations with B3LYP-D3 and B3LYP showed notable differences in aryl-Au and aryl-Cl distances (Table S2), shorter for B3LYP-D3 as expected for the large contribution of dispersion in interactions of this nature.[10] Then, new calculations were made using ωB97X-D, considered to be better for long range distances.[11] These calculated structures are submitted only to intramolecular forces. Direct comparison of all the X-ray *vs.* gas phase DFT optimized structures is available as SI (Figure S2). As in the X-ray structures, there are calculated structures more symmetric (all the Cy complexes) and less symmetric (all the Ph complexes). This not always coincides with their X-ray cases (Figure 4, structures at the left). It looks that the less regular structural behavior of the DFT optimized Ph series is caused by different rotational arrangements of the aryls.

A consequence for structures being strongly asymmetric (as in [AuCl(**PhJ**)], **1**, **3**, and **5**), is that the Au–Cl moiety interacts preferentially with one half of the distal aryl and differently with the other half. Note, however, that there is another source of asymmetry. Figure 4 shows the molecules viewed in the direction of an imaginary line connecting Au to C^1 (C^1 is eclipsed below the Au atom). This view does not make evident the existence of tilting of the distal aryls (present as well in the asymmetric complexes), also bringing one half of this ring closer to the Au–Cl moiety than the other half. In fact, the Au–C^2 *vs.* Au–C^6 (see Table 2, columns 3 and 4), or Cl–C^3 *vs.* Cl–C^5 distances (see later in the topological analysis of the Cl region), are always different, even in the most symmetric Cy family.

Table 2. Calculated Au–C distances (Å) and Au charges (au) for gas phase DFT optimized [AuCl(L^n)] structures.

Complex	Au-C^1	Au-C^2	Au-C^6	Au charge
AuCl(**PhJ**) (PhHH)	3.351	3.399	3.696	0.132
AuCl**L**^{1} (PhHF)	3.289	3.388	3.536	0.123
AuCl**L**^{3} (PhFH)	3.258	3.360	3.559	0.147
AuCl**L**^{5} (PhFF)	3.199	3.312	3.451	0.137
AuCl(**CyJ**) (CyHH)	3.287	3.393	3.515	0.112
AuCl**L**^{2} (CyHF)	3.233	3.363	3.432	0.099
AuCl**L**^{4} (CyFH)	3.237	3.391	3.436	0.123
AuCl**L**^{6} (CyFF)	3.193	3.330	3.423	0.107

The distances in Tables 1 and 2 confirm that, as expected, all the DFT optimized distances are longer than the corresponding experimental lengths. This structural breathing is a familiar phenomenon.[12] It is worth noting that, once the crystal forces are absent, the calculated molecular structures show almost identical Au–P and the Au–Cl distances (within 0.01 Å) for the whole series of complexes (Table S2, calculated). In contrast, the Au–C differences associated to atoms with weak Au–C interactions are clearly larger, in the order of 0.1 Å (Table 2, columns 2 and 3).

We start our analysis of calculated gas phase structures in the zone closer to gold. Rather than using the aryl "hapticity" number proposed by Kochi,[13] we prefer to examine individually the Au–C distances given in Table 2. All the Au–C^1 distances are shorter than their corresponding Au–C^2 or Au–C^6 distances. Thus, the weak interactions seem to involve more significantly C^1 in all cases. Then, Au–C^2 is shorter than Au–C^6 for **1**, **3**, and **5**, and the same applies to **2**, **4**, and **6** but with more similar less different distances to the two ortho carbon atoms. Thus, the geometrical asymmetry commented above seems to be an important factor for the distance differences in **1**, **3**, and **5**, and the tilting effect is smaller.

Since Au-C^1 are the most significant interactions, the values in Table 2 column 2 should be carefully considered. The sequence of distances in the Cy family immediately shows an order of distances HH > FH > HF > FF that makes sense if the influence of fluorination to produce shorter distances is high in the distal aryl, and much less but not negligible in the proximal aryl. This is not so well defined for the less regular Ph family, due to the structural variations mentioned. For this reason, the more symmetric Cy series provides more valuable information for structure/properties analysis. Yet, the two FF complexes, **5** and **6**, show the two shortest Au–C^1 calculated distances. The gold atoms show positive Bader charges in the range 0.123-0.147 atomic units for the Ph

family of phosphines, and 0.099-0.123 au for the complexes with the more donor Cy phosphines (Table 2, last column). In the Cy series the HF and FF complexes coincide to have the lower positive Au charges and, however, produce the shortest Au-C^1 distances.

What do we call weak interactions?

An interesting study of biaryl phosphine gold(I) cationic $[Au\{PR_2(biaryl)\}(arene)]^+$ complexes provides information on covalent Au^I–arene bond distances trans to P. The study concludes that *significant interactions with arenes should show distances of less than 2.95 Å for* Au^I.[4d] Obviously, the words "*significant interactions*" mean covalent interactions involving positive orbital overlapping and net charge transfer between atoms. Above this distance (2.95 Å), calculations *indicate conclusively that no electron transfer occurs from the arene to the metal and that the interaction does not have any covalent character.*[4d] Taking 2.95 Å as the "bond" limit for gold(I) and arenes, moving beyond 2.95 Å from Au, we are getting into the "beyond bond" domain. According to the values in Table 2, the later condition fully applies to the biphenyl moiety of the PR_2(biaryl) ligands. There we speak of "*weak interactions*", "no-bond" interactions, or non-covalent interactions (NCI). These interactions include attractive and repulsive electrostatic interactions, dipole inductions (polarizations), and attractive interactions between instantaneous multipoles (London dispersion) and, as a whole, are often referred to as van der Waals (vdW) forces. The name "closed-shell" is also applied to them by contrast with the "shared-shell" (covalent) interactions.[14]

The vdW radius is well defined for simple entities not prone to exchange electron density, as in the case of two contacting noble gas atoms. In any other circumstance (even in simple molecules) this *ideal* concept is contaminated by the presence of other influences (*e.g.* implication of these atoms in covalent bonds that will alter their spherical electron density distribution, which becomes no more spherical, or any other intra- or intermolecular forces). Depending on the direction chosen to define the vdW distance to other atoms or molecules, the molecular and atomic deformations will affect the measurement. This means that well defined values for *ideal* vdW radii cannot be experimentally afforded.

Another point is that the vdW interatomic interactions are very weak at their *ideal* vdW distances and, consequently, any significant external force can overcome them, shortening the original interatomic distance and produce a significant increase of the non-covalent interactions' strength. Similarly, any forced lengthening will weaken the interaction significantly. In any real system, the equilibrium vdW distance observed should be the distance at which the compressive external forces and those opposing compression are compensated. Many external forces work for compression. Specifically, the structural compression mentioned above for X-ray structures is the complex balance of a summation of inter- and intramolecular interactions plus the tendency to achieve good occupancy of space. In gas-phase molecular calculations, only intramolecular interactions are operative.

As initial guess and first reference, the expected distance between two contacting atoms submitted to vdW forces is obtained by the sum of their tabulated vdW radii. Different tables of vdW radii (Bondi,[9] Batsanov,[15] Alvarez[16]) are available in the literature. Taking the most used values proposed by Bondi, the expected Au–C vdW distance is 3.36 Å. The vdW radii of Batsanov would bring this distance to 3.87 Å. It is out of discussion that even using the 3.36 Å value, the Au–C^1 and Au–C^2 distances in Table 2, are significantly shorter (*e.g.* 3.066 and 3.237 in complex **4**). It makes sense to ask why, in the isolated molecule and in the absence of covalent Au–C interactions, the biphenyl ring still chooses to get so close to gold (structure **A** in Figure 5), forcing the ligand to adopt unnatural bending angles (15-20°) between the Au–P and the inter-ring C_{ipso}–C^1 bond lines,[4c] as well as "no bond" distances shorter than the sum of vdW radii, instead of taking any other orientation not requiring structural distortion of the ligand (*e.g.* **B** in Figure 4**B**).

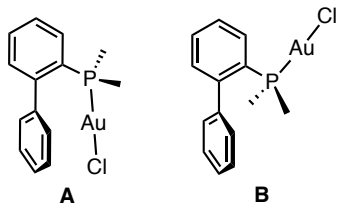

Figure 5. Alternative structures with (**A**) and without (**B**) Au-C^1 short distance.

The thermodynamic net stabilization of structure **A** *vs.* **B** was calculated for all the $[AuCl\{PR_2(biaryl)\}]$ complexes of this study affording values in the range 1-10 kcal×mol^{-1} (Table 3). This coincides fairly well with other stabilization values recently reported for 25 PR_2(biaryl) non-fluorinated ligands (around 7.2 (±3.3) kcal×mol^{-1} for the whole series).[6] For structure **A** to be the preferred thermodynamic result, the "weak interactions", certainly enhanced at the shorter distances observed, should compensate and overcome the cost of structurally forcing the ligand.

Table 3. Calculated higher stability of structure **A** vs. **B** (ΔΔG° in $kcalmol^{-1}$) for $[AuCl(L^n)]$ in gas phase.

[a]Complex	ΔΔG° A-B	Complex	ΔΔG° A-B
AuCl(**PhJ**)	–5.2	AuCl(**CyJ**)	–0.9
AuCl**L**[1] (PhHF)	–2.3	AuCl**L**[2] (CyHF)	–3.4
AuCl**L**[3] (PhFH)	–6.6	AuCl**L**[4] (CyFH)	–5.7
AuCl**L**[5] (PhFF)	–3.4	AuCl**L**[6] (CyFF)	–8.9

In our study there is a clear higher stabilization for the fluorinated Cy complexes **2**,**4**, and **6** than for their non-fluorinated reference [AuCl(**CyJ**)]. The stabilization of **A**

vs. **B** is enough to make structure **B** virtually inexistent in a putative equilibrium of the two rotational isomers. In fact, to the best of our knowledge form **B** has never been observed in these gold complexes. The adoption of structure **A** occurs with similar success for any complex, be it fluorinated or not. In order to get additional information about the F effect on the interactions existing in the zone beyond the Au–C covalent bond frontier, QTAIM studies were carried out.[17,18]

Topological analysis of the distal aryls

The Gradient Line Maps (GLM) of the distal aryls for structures **A** were examined, looking for possible effects of H and F substitution in the ligands. GLM of the distal aryl plane for all the complexes are available in Figure S3. Figure 6 compares the distal aryls of complexes [AuCl(**CyJ**)] (CyHH) and **6** (CyFF), which differ in the fluorination of the biphenyl aryl in **6**.

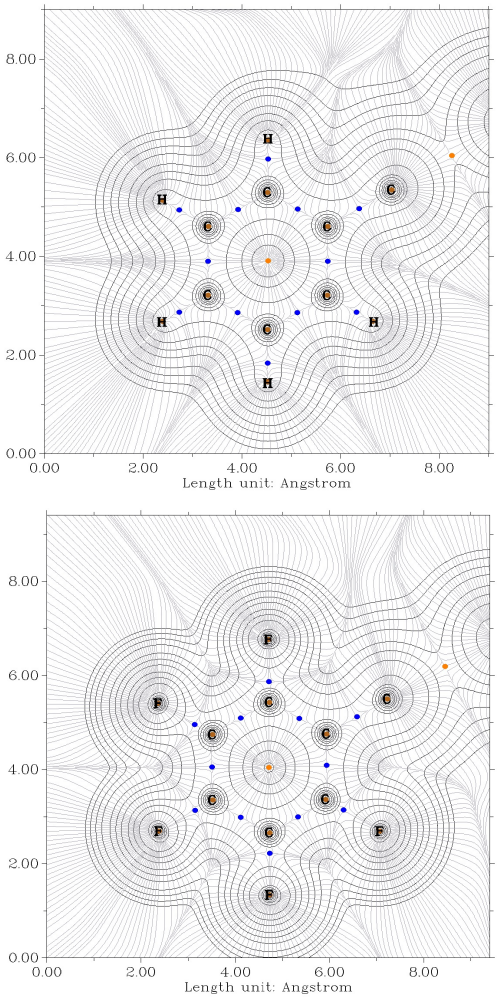

Figure 6. GLM with contour lines for the distal aryls of complexes [AuCl(**CyJ**)] (above) and [AuCl(**L**^{6})] (below). Blue dots are (3, -1) CPs and orange dots are (3, +1) CPs.

These GLM display twelve (3, -1) critical points (CP), corresponding to: the six C–C(ring) bonds; one C^1–C_{ipso} bond; and five C–H bonds, or five C–F bonds (blue); in addition, the (3, +1) ring CP (orange) appears. The positions of the bond CPs reflect clearly their polarization: the six $CP(C–C)_{ring}$ are centered, the CP(C–H) are closer to H than to the Csp^2 atom, and the CP(C–F) are much closer to the Csp^2 than to F.

The data of atomic charges provides interesting information. Table 4 summarizes this information for [AuCl(**CyJ**)] and [AuCl**L**^{6}] as representative examples. Remember that their structures are almost symmetric. The C^2-C^6, and H^2-H^6 Bader charges in [AuCl(**CyJ**)] are very close to zero (columns 2 and 3), as expected for C–C and C–H bonds of very low polarity. On the contrary, the very polar C–F bonds in [AuCl**L**^{6}] give rise to large positive charges for C^2-C^6 (about 0.59-0.67 au), and large negative charges of similar magnitude for F^2-F^6 (columns 4 and 5). For C^1, a moderate positive charge of 0.0555 au is found in [AuCl**L**^{6}], compared to the small negative charge of –0.0125 au in [AuCl(**CyJ**)], with a total variation of 0.0680 au upon H by F substitution.

Table 4. QTAIM atomic charges for structures [AuCl(**CyJ**)] (HH) and [AuCl**L**^{6}] (FF).

Atom	AuCl(**CyJ**) Charges	H^2-H^6 Charges	AuCl**L**^{6} Charges	F^2-F^6 Charges
Au	0.1121		0.1069	
Cl	-0.5989		-0.5790	
P	1.8662		1.8707	
C^1	-0.0125	–	0.0555	–
C^2	-0.0126	0.0053	0.5933	-0.6573
C^3	0.0096	0.0168	0.6507	-0.6354
C^4	0.0214	0.0247	0.6725	-0.6338
C^5	0.0102	0.0169	0.6494	-0.6360
C^6	-0.0125	0.0081	0.5944	-0.6569

Topological analysis of the gold region

The negative (or less positive) charges on C^2-C^6 carbon atoms in C-H aryls should make the π electron density of the distal aryl ring softer and more polarizable than in the complexes with C-F aryl carbon atoms with large positive charges. For the same reason, the polarizing power of these Csp^2 atoms should be lower for C–H and higher for C–F ring atoms. The effect of fluorination should be much less on C^1 (bonded to C_{ipso}), which is only indirectly affected by the F presence in the other Csp^2 atoms. Looking at the charge values in Table 4 for the two Cy complexes (-0.0125 *vs*. + 0.0555 au), there is a difference of 0.0680 au in the C^1 charges and only 0.0052 au in the Au atoms. Since the Au–C^1 distance is noticeably shorter in complex **6**, this suggests that, against initial intuition, the effect of distal aryl fluorination on carbon atoms is contracting its electronic cloud (see figure 6), thus reducing the repulsive interelectronic interactions with gold and allowing for a closer approximation of the two nuclei at attraction-repulsion equilibrium.

The eight complexes in Table 2 show the presence of two (3, -1) critical points, as displayed in the GLM of complex **1** (Figure 7): one between the two aromatic carbon atoms more involved in gold interaction, CP(C^1–C^2),

and one between the Au atom and C^1, CP(C^1–Au). It is noteworthy that the latter is placed practically on the Au···C^1 line and far from the Au···C^2 line in all the complexes, with C^1–CP–Au angles in the range 172.5-177.1°. This supports that, in the interaction between gold and the C^2–C^1–C^6 triangle, C^1 is dominant as commented above.

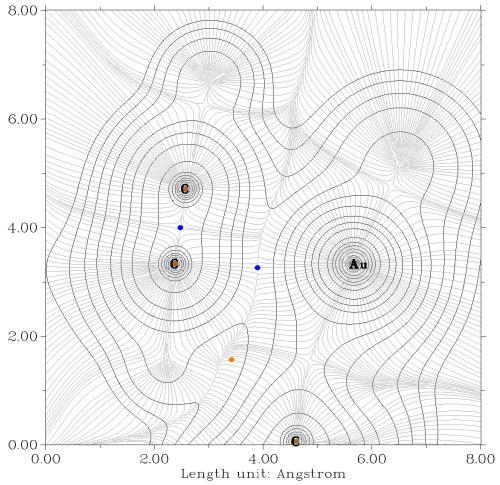

Figure 7. GLM with contour lines for complex **1**. The plane chosen is defined by Au (right), C^1 (left, below) and C^2 (left, above). Blue dots are (3, -1) CPs.

The electron density $\rho(r_{cp})$ values at the CP(C^1–C^2) (Table 5, column 2, entries 1-8) are quite high (> 0.30 au), consistent with multiple covalent bonds. In contrast $\rho(r_{cp})$ values at CP(C^1–Au) (Table 5, column 3) are extremely low (about 0.01 au), consistent with NCI contacts between C^1 and Au. Evaluation of other topological parameters, such as the Laplacian of electron density, identifies these NCI as non-covalent closed shell interactions (Table S3).[19] Similar results are found for the rest of gold complexes (Figure S4). The CP(C^1–Au) position marks the boundary of atomic domains (basins) of the two interacting atoms in the C^1-Au direction. Consequently, we can assign the C^1-to-CP and Au-to-CP distances as the corresponding *local vdW radii* of C^1 and Au under the interaction pressure (Table 5, columns 4 and 5). Both *local* radii are shorter or much shorter in all our complexes than the vdW radii values in the literature tables,[16] confirming that they are compressed in the direction of interaction, under the effect of intramolecular forces. The C atom radius shrinks to about 88% of its value in literature tables. Very interestingly, the Au^I radius shrinks more, to about 75% of its value in tables, suggesting that this gold(I) is softer (hence more polarizable) than the Csp^2 in these complexes. This is to be expected as C is a second row element with more compact orbitals. The fact that the Au–C^1 distances for the complexes are almost exactly coincident with the sum of local vdW radii is a consequence of the CP being almost exactly on the Au–C^1 line. The X-ray structure of complex **1** (Table 5, entry 9), examined as an example of solid state circumstance, is consistent with the same analysis. Its parameters afford *local* vdW radii even lower than for the molecular calculations, under the higher stress of crystal forces.

Table 5. Electron density at (3, -1) CPs (eu), and vdW contact radii (Å) in [AuCl(PR_2(biphenyl)] complexes.

Complex	$\rho(r_{cp})$ C^1–C^2	$\rho(r_{cp})$ C^1–Au	d(Å) CP-C^1	d(Å) CP-Au	Au-C^1 (Å)
AuCl(**PhJ**)	0.3095	0.0111	1.541	1.816	3.351
AuCl**L**^{1} (PhHF)	0.3138	0.0126	1.520	1.772	3.289
AuCl**L**^{3} (PhFH)	0.3105	0.0127	1.499	1.762	3.258
AuCl**L**^{5} (PhFF)	0.3152	0.0145	1.480	1.722	3.199
AuCl(**CyJ**)	0.3101	0.0120	1.518	1.772	3.287
AuCl**L**^{2} (CyHF)	0.3153	0.0136	1.494	1.740	3.233
AuCl**L**^{4} (CyFH)	0.3108	0.0129	1.492	1.747	3.237
AuCl**L**^{6} (CyFF)	0.3156	0.0145	1.475	1.719	3.193
AuCl**L**^{1} **XRay**	0.3265	0.0149	1.466	1.714	3.173

Topological analysis of the chloro region

The analysis made for the C^1–C^2–C^6 part of the distal aryl, contacting Au at short distances preferentially with C^1, finds very different circumstances at the opposite side of this ring, for C^3–C^4–C^5 and the chloro ligand. First of all, the interactions of the C atoms (C^4 for the symmetric complexes) and the chloro ligand are at a larger distance, imposed by the non-parallel arrangement of the aryl and the Au–Cl bond. At variance with the Au–C distances, all the Cl–C distances in the optimized gas phase structures (Table 6) are longer than the sum of vdW radii (3.45-3.52 Å depending on the literature table used).[16]

Table 6. Calculated Cl-C^3, Cl-C^4, and Cl-C^5 distances (Å) for DFT optimized [AuCl(L^n)] gas phase structures, and chloro charges. * Shorter distance in each complex.

Complex	Cl–C^3	Cl–C^4	Cl–C^5	Cl charge
AuCl(**PhJ**)	3.969*	4.328	4.938	-0.591
AuCl**L**^{1} (PhHF)	3.703*	3.830	4.409	-0.578
AuCl**L**^{3} (PhFH)	3.851*	4.162	4.761	-0.583
AuCl**L**^{5} (PhFF)	3.752	3.590*	3.752	-0.572
AuCl(**CyJ**)	4.056	3.793*	4.093	-0.599
AuCl**L**^{2} (CyHF)	3.832	3.564*	3.882	-0.585
AuCl**L**^{4} (CyFH)	3.954	3.718*	4.052	-0.593
AuCl**L**^{6} (CyFF)	3.784	3.526*	3.846	-0.579

The gold complexes with fluorinated ligands show shorter distances of the chloro ligand to the two closer C atoms (C^4 or C^3) than in the reference H complexes [AuCl(**PhJ**)] and [AuCl(**CyJ**)]. A regular sequence of Cl–C^4 distances HH > FH > HF > FF is found for the Cy family. For the Ph ligands, the shorter distances are to C^3, with one exception (**5**).[20] The molecules with ligands having two fluorinated aryls, **5** and **6**, show the shortest distances in their series.

The main difference with the Au/Csp^2 interactions is that in the Cl/Csp^2 case the C^4 or C^3 atoms involved have very small charges close to zero for the CH atoms, but

large positive charges (> 0.65 au) for the CF atoms (Table 4), which confers them a highly polarizing potential. Furthermore, instead of Au with positive charge, the chloro ligand shows a large negative charge in the range 0.572–0.599 au (Table 6). The larger values are for the complexes with the more donor ligands, **CyJ** and **PhJ**, but the complexes with fluorinated ligands still show highly negative Cl charges.

In this zone of weak interactions at large distances, a polarization of the π-electron density of the aryl is not conceivable, since Cl shows negative charge. On the contrary, this negative charge will contribute to make the Cl electron density softer, facilitating a more efficient polarization by the positive Csp^2. Maybe this contribution is small due to the long distances, but it is expected to be larger in the complexes with fluorinated ligands where the positive charges of C^3 or C^4 are 10 times larger.

Maps of the Cl-C^3-C^4 plane for all the complexes are available in Figure S5. The Cl–C critical points are being missed for the complexes with non-covalent interactions at larger distances (*e.g.* complex **1**), but critical points Cl–C^4 were localized for the complexes with ligands $\mathbf{L^5}$, **CyJ**, $\mathbf{L^2}$, $\mathbf{L^4}$ and $\mathbf{L^6}$ (*e.g.* complex **6** in Figure 8).

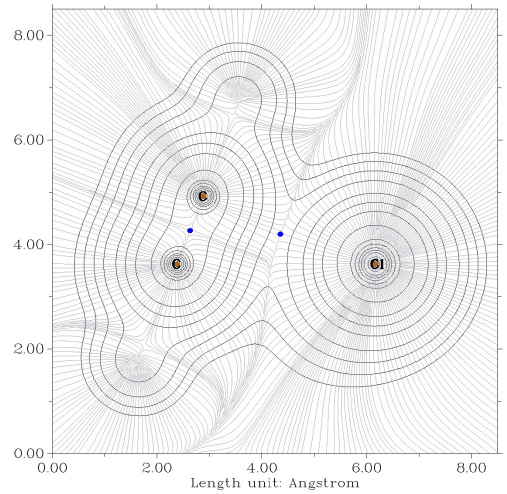

Figure 8. GLM with contour lines in the Cl(right)-C^3(left, below)-C^4(left, above) plane of **6**, showing one (3,-1) CP(Cl–C^4).

Table 7 collects the electron density at some bond and no-bond critical points CPs and, more interesting, the distances from the critical point to the corresponding C or Cl atom, CP-Cl and CP-C^4. As in the gold zone, these are assigned as *local* vdW radii. The CP–Csp^2 distances are all within a reasonably narrow range (1.650–1.805 Å) not far from the literature vdW radius for C (1.7-1.75 Å), but the CP–Cl distances (1.905–2.073 Å) are noticeably larger than the literature vdW radius for Cl (1.75 Å for Bondi; 1.8 Å for Batsunov; 1.82 Å for Álvarez). As expected, the softer Cl electron density assumes most of the polarization in this interaction and its *local* vdW radius is clearly expanded in the Cl···C^4 direction. This is perceived in the GLM (Figure 8). The fact that the shortest Cl–C^4 distances are found for the complexes **2**, **5**, and **6** (Table 6), with pentafluorophenyl as distal aryl, fits well with the much higher positive charge of C^4 in these complexes.

Table 7. Electron density at CPs, and CP-Cl and CP-C^4 distances. $CP_{Cl\text{-}C4}$ was not found for [AuCl(**PhJ**)], **1** and **3**.

Complex	$\rho(r_{cp})$ C^3–C^4	$\rho(r_{cp})$ C^4–Cl	d(Å) CP-Cl	d(Å) CP-C^4
AuCl(**PhJ**)	0.3148	-	-	-
AuCl$\mathbf{L^1}$ (PhHF)	0.3237	-	-	-
AuCl$\mathbf{L^3}$ (PhFH)	0.3142	-	-	-
AuCl$\mathbf{L^5}$ (PhFF)	0.3235	0.0058	1.940	1.689
AuCl(**CyJ**)	0.3144	0.0044	2.073	1.805
AuCl$\mathbf{L^2}$ (CyHF)	0.3235	0.0059	1.929	1.669
AuCl$\mathbf{L^4}$ (CyFH)	0.3146	0.0049	2.015	1.761
AuCl$\mathbf{L^6}$ (CyFF)	0.3234	0.0063	1.905	1.650
AuCl$\mathbf{L^1}$ XRay	0.3449	0.0059	1.955	1.759

Non-covalent interaction analysis (NCI)

Since the meaning of QTAIM analysis has been sometimes disputed when particularly weak non-covalent atomic interactions are involved, as it is the case, we have performed a noncovalent interaction analysis (NCI),[21,22] to visualize the clash zones and get a tridimensional picture of the interactions between the Au–Cl zone and the distal-aryl. As an example, we take in the text the representative cases complexes **1** for the asymmetric structure and **2** for the more symmetric structure. For all the complexes, see figures S6-S8 in SI. The plot of reduced density gradient vs. $\text{sign}(\lambda_2)\rho$ for the asymmetric complex [AuCl$\mathbf{L^1}$] (**1**) (Figure S6) shows the presence of van der Waals interactions ($-0.01 < \text{sign}(\lambda_2)\rho < -0.005$) along with steric repulsions ($\text{sign}(\lambda_2)\rho > 0.005$), mainly associated to the aryl rings. More visual, the green-brown colored gradient isosurface (Figure 9) shows a continuous of attractive and repulsive weak interactions, spanning from C^1 to C^4, between the pentafluorophenyl distal ring and the Au–Cl fragment.

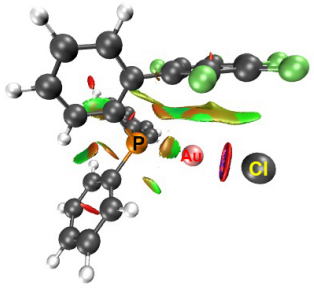

Figure 9. Gradient isosurface (s = 0.5 au) for **1**, colored on a blue-green-red scale according to values of $\text{sign}(\lambda_2)\rho$, ranging from -0.04 to 0.02 au. Green: weak attractive interactions; red: strong non-bonding overlap.

Reducing the s value from s = 0.5 au to s = 0.35 au (Figure 10, left), and examining the gradient surface from above the pentafluorophenyl ring (Figure 9, right), provides a more informative view and allows to identify two areas of higher interaction: one that confirms concentration of weak attractive interaction in the Au/C^1/C^2 zone,

and another that recognizes weak attraction forces focused in the Cl/C^3/C^4 one. This separation in two zones is in part an artifact provoked on purpose to facilitate the analysis. The truth is that each molecular component has an influence on the others, and the structural equilibrium (distances), as well as the charges and electronic density at each point are the result of the global effect of many concerted interactions. This explains again why it is not possible to achieve precise correlations when comparing individual local magnitudes observed in the DFT and QTAIM studies (e.g. distances to gold) and local data (e.g. charges on gold).

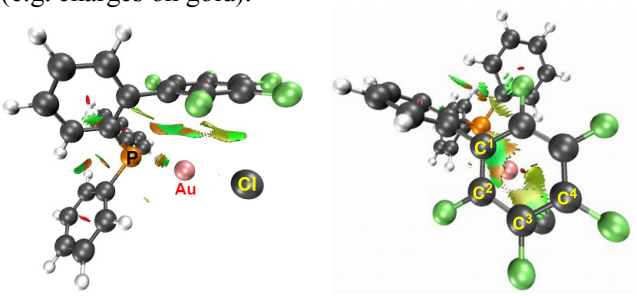

Figure 10. Two views of the gradient isosurface (*s* = 0.35 au) for complex **1**. Same color codes as in Figure 9.

Figure **11** allows to compare directly asymmetric *vs*. symmetric (above *vs*. below) and non-fluorinated *vs*. fluorinated (left *vs*. right) in the complexes [AuCl(**PhJ**)], [AuCl(**L**^{1})] (**1**), [AuCl(**CyJ**)], and [AuCl(**L**^{2})] (**2**).

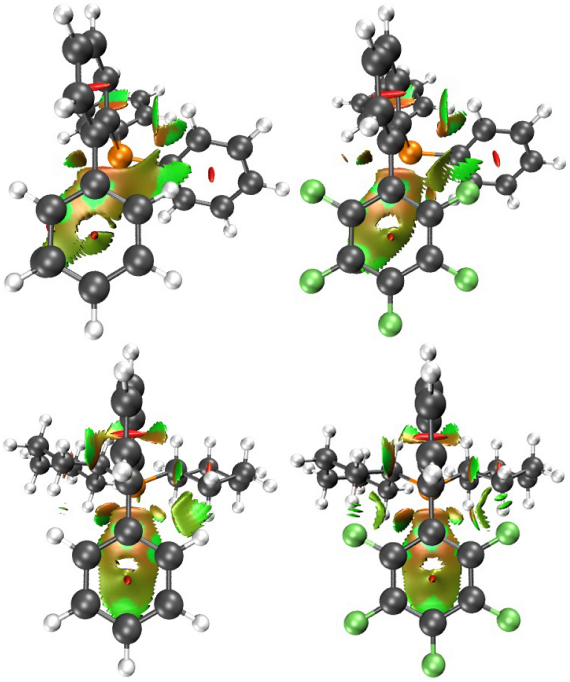

Figure 11. Gradient isosurfaces (*s* = 0.50 au) of [AuCl(**PhJ**)] (above left), **1** (above, right), [AuCl(**CyJ**)] (below, left), and **2** (below, right). Viewed along the Au···C^1 imaginary line (Au is eclipsed by the C^1 above it)**.**

It can be noted that for the symmetric Cy complexes, the C^4 interactions with Cl (this atom is hidden behind the gradient isosurface) and the C^1 interactions with Au are, according to the color code, apparently well-defined for the non-fluorinated [AuCl(**CyJ**)] (below, left), and for **2** (below, right). For the less symmetric [AuCl(**PhJ**)] (above left) and **1** (above, right) the asymmetry seems particularly detrimental for the Cl–C^4 interaction, in favor of Cl–C^3.

NBO analysis

The results discussed so far provide information on atomic properties (e.g. charges and distances). However, the NCI forces involve electron densities and dipolar moments rather than individual atoms, and a further analysis can be more helpful for this. In order to have an approximate estimation of the energy of these non-covalent interactions, we have carried out an NBO analysis (Table 8 for the Cy complexes; the whole set of NBO results is given in Table S4).

Table 8. Donor and acceptor NBOs and E_{SOPT} values (kcal×mol^{-1}) for ring interactions with Au (values above 0.5) and with Cl (values above 0.05), for the symmetric complexes [AuCl(**CyJ**)], [AuCl**L**^{2}], [AuCl**L**^{4}], and [AuCl**L**^{6}].

[AuCl(**CyJ**)]		
Donor NBO	Acceptor NBO	E_{SOPT}
24. BD(1) C^1-C^2	102. LP*(8) Au	1.66
25. BD(1) C^1-C^6	102. LP*(8) Au	1.47
34. BD(1) C^2-C^3	102. LP*(8) Au	0.92
35. BD(2) C^2-C^3	101. LP*(7) Au	0.55
37. BD(1) C^4-C^5	102. LP*(8) Au	0.76
39. BD(1) C^4-C^3	102. LP*(8) Au	0.79
47. BD(1) C^5-C^6	102. LP*(8) Au	0.83
104. LP(2) Cl	513. BD*(2) C^4-C^5	0.14

[AuCl**L**^{2}]		
Donor NBO	Acceptor NBO	E_{SOPT}
29. BD(1) C^1-C^6	107. LP*(8) Au	2.05
31. BD(1) C^1-C^2	107. LP*(8) Au	1.87
39. BD(1) C^6-C^5	107. LP*(8) Au	1.51
40. BD(1) C^4-C^3	107. LP*(8) Au	1.20
41. BD(1) C^4-C^5	107. LP*(8) Au	1.32
49. BD(1) C^3-C^2	107. LP*(8) Au	1.28
109. LP(2) Cl	534. BD*(1) F^4-C^4	0.10
109. LP(2) Cl	562. BD*(2) C^4-C^5	0.15
110. LP(3) Cl	562. BD*(2) C^4-C^5	0.11

[AuCl**L**^{4}]		
Donor NBO	Acceptor NBO	E_{SOPT}
25. BD(1) C^1-C^6	106. LP*(8) Au	1.60
26. BD(2) C^1-C^6	106. LP*(8) Au	0.52
27. BD(1) C^1-C^2	106. LP*(8) Au	1.58
34. BD(1) C^6-C^5	106. LP*(8) Au	0.89
36. BD(1) C^4-C^3	106. LP*(8) Au	0.83
37. BD(1) C^4 -C^5	106. LP*(8) Au	0.80
46. BD(1) C^3- C^2	106. LP*(8) Au	0.91
47. BD(2) C^3-C^2	105. LP*(7) Au	0.64
108. LP(2) Cl	549. BD*(2) C^4-C^5	0.19

[AuCl**L**^{6}]		
Donor NBO	Acceptor NBO	E_{SOPT}
30. BD(1) C^1-C^6	111. LP*(8) Au	2.06
32. BD(1) C^1-C^2	111. LP*(8) Au	1.84
39. BD(1) C^6-C^5	111. LP*(8) Au	1.50
40. BD(1) C^4-C^3	111. LP*(8) Au	1.14
41. BD(1) C^4-C^5	111. LP*(8) Au	1.28
49. BD(1) C^3-C^2	111. LP*(8) Au	1.23
113. LP(2) Cl	574 . BD*(1) F^4-C^4	0.06
113. LP(2) Cl	598. BD*(2) C^4-C^5	0.07
114. LP(3) Cl	574. BD*(1) F^4-C^4	0.08
114. LP(3) Cl	598. BD*(2) C^4-C^5	0.23

As expected, all the E_{SOPT} contributions are very small, compared to the values for covalent bonds. Altogether, for Au they implicate electron density of the whole ring, showing that the geometrical assignment of hapticity h^x labels is electronically less meaningful. The stronger interactions correspond systematically to several π-bond donations from the ring to an empty (99.4% p) orbital of gold. With a threshold of 0.5 kcal×mol^{-1}, several contributions are found in the overall range 2.06-0.55 kcal×mol^{-1}. NBOs representing potential donations from Au to aryl BD* orbitals are not found, meaning that this kind of interaction is less significant.

The C-C bonds involved in the aryl-gold interaction reflect well the symmetric (Table 8) or more asymmetric (Table S4) molecular structure, and also the preferred tilting of the aryl (C^2 *vs*. C^6). The bonds C^1-C^6 and C^1-C^2 are always present and usually dominant in the interaction with gold, but others are important too, even in the more symmetric molecules. See for instance 30-49 donor NBOs in complex [AuCl**L^6**], showing significant involvement of electron density associated to $C^{1,2,3,4,5,6}$. The overall energy of interaction with gold, taken as the sum of the contributions in Table 8, is clearly a function of the fluorination or not of the distal aryl: this sum is 6.98 for [AuCl(**CyJ**)] (HH) and 6.97 for [AuCl**L^4**] (FH), but 9.23 for [AuCl**L^2**] (HF) and 9.05 for [AuCl**L^6**] (FF).

On the other hand, LP Cl (99.4-99.8% p) donations, not only to BD* C-C but also to BD*F–C bonds are found (see 574 in [AuCl**L^6**]). These interactions are weak but not insignificant. With a threshold of 0.05 kcal×mol^{-1}, a few contributions are found in the overall range 0.23-0.06 kcal×mol^{-1}. Again, the overall energy of interaction with chloro, taken as the sum of the contributions in Table 8, is clearly a function of the fluorination or not of the distal aryl, and a similar sequence is found for the aryl-Cl [AuCl**L^6**] interactions: 0.14 for [AuCl(**CyJ**)] (HH) and 0.19 for [AuCl**L^4**] (FH) vs. 0.36 for [AuCl**L^2**] (HF) and 0.44 for [AuCl**L^6**] (FF). That is about 5% compared to gold.

For the whole series, the sum of computed E_{SOPT} is in the range 2-10 kcal×mol^{-1}, which is very consistent with the computed values for the difference in stability between structures **A**, where these NCIs exist, and the structures **B**, where they have been broken.

In summary, in the distal-aryl/Au-Cl zone of the [AuCl{PR_2(biaryl)}] complexes, the interactions with gold occur at distances shorter than the sum of vdW radii, whereas the interactions with Cl occur at distances larger than the sum of vdW radii. Consequently, the non-covalent interactions holding the aryl attached to the Au–Cl fragment consist mostly of a significant polarization of the π-aryl electron density (not only that involving C^1) by gold, and a Cl polarization by the aryl carbons atoms, weaker but still operating at larger distance. The overall balance of interactions is significantly stronger, and the vdW distances shorter, for the phosphines with a fluorinated distal aryl creating higher charges on the aryl C^2-C^6 carbon atoms.

CONCLUSIONS

Our results show that for [AuCl(PR_2(biaryl)] complexes the observed structures **A** are energetically preferred to the non-observed alternative **B** by less than 10 kcal×mol^{-1}. The fluorination at the distal aryl gives rise to the appearance of strong dipoles and produces some contraction of the π-aryl electron cloud. This favors stronger vdW interactions with both zones (Au–C and Au–Cl) at shorter distances than for H distal aryls.

QTAIM and NCI methods clearly identify these "no-bond" interactions at distances shorter than the Au–C sum of vdW radii, for the Au zone, but also at larger distances than the sum of C and Cl vdW radii, in the Cl zone. NBO examination of these NCIs complexes confirms stronger interactions in the case of fluorinated aryls, mostly due to the enhancement of aryl–Au forces. When the small E_{SOPT} values are transported to analyze the weak interactions in discussion, it is important to be aware that attractive and repulsive forces are less obvious in NCI systems than in covalent systems. The enhancement of these interaction can be propitiated by the decrease of repulsive interactions as much as by the increase of attractive interactions. Fluorination of the C atoms seems to produce its positive effect due to polarization of the aryl electronic cloud towards the F substituents, thus diminishing the repulsive forces with the electronic cloud of gold and allowing for shorter Au–C distances.

In a different field, this study suggests that some differences, probably not very dramatic, might be expected in catalysis with gold complexes using these fluorinated phosphines instead of the popular hydrogenated ones. In these catalysis Cl^- is usually extracted with a soluble silver salt, and the coordination position of Cl in the cationic catalyst is occupied successively by ancillary ligands or by the reagent to be activated. Since the distal F–C^4 atom exert a higher polarizing effect in this coordination zone than H–C^4, it makes sense that the phosphines perfluorinated in the distal aryl might exert some influence, particularly on easily polarizable reagents such as olefins. A less hypothetical case, already in study, is Pd catalysis,[7] where the Pd-distal aryl interactions are covalent bonds and play a much more important role.

EXPERIMENTAL SECTION

General considerations. All the manipulations were performed under N_2 atmosphere using standard Schlenk techniques. Solvents were dried using a solvent purification system SPS PS-MD-5 or distilled from appropriate drying agents.[23] $CDCl_3$ for phosphine characterization was vacuum-transferred from CaH_2 and degassed using freeze-pump-thaw technique. Commercially available chemicals were purchased from Sigma Aldrich, Alfa

Aesar, Fluorochem and Acros Organics and were used without further purification. [AuCl(tht)],[24] 2'-bromo-2,3,4,5,6-pentafluoro-1,1'-biphenyl,[25] 2-bromo-3,4,5,6-tetrafluoro-1,1'-biphenyl,[26] 2-bromo-2',3,3',4,4',5,5',6,6'-nonafluoro-1,1'-biphenyl,[27] 2',3',4',5',6'-pentafluoro-[1,1'-biphenyl]-2-yl)diphenylphosphine (L^1)[7] were prepared by reported methods. Flash chromatography was carried out using silica gel (230-240 mesh) and oxygen-free solvents. Chemical yields refer to pure isolated substances. NMR spectra were recorded with Bruker Avance 400 Ultrashield and Varian 500/54 Premium Shielded instruments equipped with variable-temperature probes. Chemical shifts are reported in ppm referenced to tetramethylsilane (^{1}H), CCl_3F (^{19}F), and 85% H_3PO_4 (^{31}P), with positive shifts downfield, at 298 K unless otherwise stated. HRMS (EI) were performed with a MALDI Bruker Autoflex at the LTI facilities of Valladolid University (Spain). Elemental analysis were carried out with a Carlo Erba 1108 Elemental Analyzer at the services of Vigo University (Spain).

Synthesis of phosphines. General procedure. A flame-dried, nitrogen-purged Schlenk flask was charged with the corresponding bromo-biphenyl (1.55 mmol, 1 eq) and 12 mL of dry Et_2O. The resulting solution was cooled to -78 °C and a 1.6 M solution of Li(*n*-Bu) in *n*-hexane (0.97 mL, 1.55 mmol, 1 eq.) was added dropwise. After stirring for 1 h, Cy_2PCl (0.38 mL, 1.70 mmol, 1.1 eq) or Ph_2PCl (0.31 mL, 1.70 mmol, 1.1 eq) was added to the reaction mixture and stirred for another 1 h. Then, the temperature was raised to -50 °C and kept at that temperature until disappearance of the starting bromo-biphenyl (monitored by TLC, 48-72 h).[28] The reaction was quenched with a deoxygenated saturated solution of $(NH_4)Cl$ and subsequently it was slowly warmed to 25 °C. The organic layer was separated, and the aqueous layer was extracted with Et_2O (4 x 6 mL). The combined organic extracts were dried over anhydrous $MgSO_4$, filtered, and the solvents of filtrate were removed under reduced pressure. The residue was purified by column chromatography on silica gel using *n*-hexane or a mixture of *n*-hexane/CH_2Cl_2 (20:1) as eluent. A colorless solid was obtained by recrystallization from *n*-hexane/ethanol.

Dicyclohexyl(2',3',4',5',6'-pentafluoro-[1,1'-biphenyl]-2-yl)phosphine (L^2). This compound was obtained from 2'-bromo-2,3,4,5,6-pentafluoro-1,1'-biphenyl (0.500 g, 1.55 mmol) and Cy_2PCl (0.38 mL, 1.70 mmol). It was purified by column chromatography using *n*-hexane/CH_2Cl_2 (20:1) and recrystallized from *n*-hexane/ethanol to obtain a colorless solid (319.2 mg, 47 % yield). **HRMS (EI)** Calculated for $C_{24}H_{26}F_5P$ $[M-F]^+$: 421.1703. Experimental $[M-F]^+$: 421.1698. **^{1}H NMR** (399.86 MHz, $CDCl_3$) δ 7.68–7.61 (m, 1H), 7.51–7.41 (m, 2H), 7.25–7.20 (m, 1H), 1.89–1.78 (m, 2H), 1.77–1.57 (m, 8H), 1.57–1.47 (m, 2H), 1.29–1.12 (m, 6H), 1.09–0.96 (m, 4H). **^{19}F NMR** (376.18 MHz, $CDCl_3$) δ -138.50 to -138.87 (m, 2F), -155.87 (t, *J* = 21.0 Hz, 1F), -162.91 to -163.20 (m, 2F). **^{31}P NMR** (161.87 MHz, $CDCl_3$) δ -6.92 (t, *J* = 24.3 Hz). **^{13}C NMR** (100.55 MHz, $CDCl_3$) δ 143.8, 140.7, 137.4, 136.7(d, *J* = 21.2 Hz), 133.3 (d, *J* = 3.6 Hz), 130.7 (d, *J* = 6.0 Hz), 129.0 (d, *J* = 1.3 Hz), 128.7, 34.1 (d, *J* = 12.6 Hz), 30.2 (d, *J* = 17.3 Hz), 28.7 (d, *J* = 7.9 Hz), 27.2 (d, *J* = 14.9 Hz), 27.1 (d, *J* = 10.3 Hz), 26.3 (d, *J* = 1.2 Hz). (Fluorine-bonded carbon shifts were determined by ^{13}C-^{19}F HSQC. Signals are expected to be doublets with $J^1_{C-F} > 220$ Hz).

Diphenyl(3,4,5,6-tetrafluoro-[1,1'-biphenyl]-2-yl)phosphine (L^3). This compound was obtained from 2-bromo-3,4,5,6-tetrafluoro-1,1'-biphenyl (0.473 g, 1.55 mmol) and Ph_2PCl (0.31 mL, 1.70 mmol). It was purified by column chromatography using *n*-hexane/CH_2Cl_2 (20:1) and recrystallized from *n*-hexane/ethanol to obtain a colorless solid (467.7 mg, 74 % yield). **HRMS (EI)** Calculated for $C_{24}H_{15}F_4P$ $[M+H]^+$: 411.0920. Experimental $[M+H]^+$: 411.0924. **^{1}H NMR** (399.86 MHz, $CDCl_3$) δ 7.44–7.37 (m, 3H), 7.34–7.27 (m, 10H), 7.20–7.15 (m, 2H). **^{19}F NMR** (376.18 MHz, $CDCl_3$) δ -121.72 (tdd, *J* = 21.9, 13.4, 7.2 Hz, 1F), -138.48 (dddd, *J* = 22.9, 12.9, 9.5, 2.9 Hz, 1F), -151.79 (ddd, *J* = 22.4, 19.9, 7.2 Hz, 1F), -154.83 (ddt, *J* = 23.7, 20.0, 3.7 Hz, 1F). **^{31}P NMR** (161.87 MHz, $CDCl_3$) δ -16.16 (ddd, *J* = 21.9, 9.4, 4.3 Hz, 1P). **^{13}C NMR** (100.55 MHz, $CDCl_3$) δ 149.6, 144.8, 141.7, 140.1, 135.0 (dd, *J* = 12.3, 2.9 Hz), 132.6 (dd, *J* = 20.3, 1.8 Hz), 130.4 (d, *J* = 3.7 Hz), 128.7, 128.7, 128.5, 128.4, 128.1. (Fluorine-bonded carbon shifts were determined by ^{13}C-^{19}F HSQC. Signals are expected to be doublets with $J^1_{C-F} > 220$ Hz).

Dicyclohexyl(3,4,5,6-tetrafluoro-[1,1'-biphenyl]-2-yl)phosphine (L^4). This compound was obtained from 2-bromo-3,4,5,6-tetrafluoro-1,1'-biphenyl (0.473 g, 1.55 mmol) and Cy_2PCl (0.38 mL, 1.70 mmol). It was purified by column chromatography using *n*-hexane/CH_2Cl_2 (20:1) and recrystallized from *n*-hexane/ethanol to obtain a colorless solid (513.0 mg, 78 % yield). **HRMS (EI)** Calculated for $C_{24}H_{27}F_4P$ $[M]^+$: 422.1781. Experimental $[M]^+$: 422.1797. **^{1}H NMR** (499.73 MHz, $CDCl_3$) δ 7.45–7.40 (m, 3H), 7.14–7.10 (m, 2H), 2.26–2.17 (m, 2H), 1.78–1.60 (m, 8H), 1.49–1.41 (m, 2H), 1.32–0.94 (m, 10H). **^{19}F NMR** (470.14 MHz, $CDCl_3$) δ -125.63 to -125.82 (m, 1F), -137.65 to -137.79 (m, 1F), -153.32 to -153.47 (m, 1F), -156.28 (ddt, *J* = 23.8, 20.2, 3.5 Hz, 1F). **^{31}P NMR** (161.87 MHz, $CDCl_3$) δ -2.36 (d, *J* = 22.0 Hz, 1P). **^{13}C NMR** (125.69 MHz, $CDCl_3$) δ 149.6, 144.9, 140.9, 139.4, 133.46, 130.84 (d, *J* = 3.5 Hz), 128.19, 127.83, 34.71 (dd, *J* = 14.0, 5.5 Hz), 31.86 (d, *J* = 22.7 Hz), 30.75 (d, *J* = 8.2 Hz), 27.06 (d, *J* = 7.7 Hz), 26.76 (d, *J* = 13.7 Hz), 26.14 (Fluorine-bonded carbon shifts were determined by ^{13}C-^{19}F HSQC. Signals are expected to be doublets with $J^1_{C-F} > 220$ Hz).

Diphenyl(perfluoro-[1,1'-biphenyl]-2-yl)phosphine (L^5). This compound was obtained from 2-bromo-2',3,3',4,4',5,5',6,6'-nonafluoro-1,1'-biphenyl (0.612 g, 1.55 mmol) and Ph_2PCl (0.31 mL, 1.7 mmol). It was

purified by column chromatography using *n*-hexane and recrystallized from *n*-hexane/ethanol to obtain a colorless solid (547.9 mg, 71 % yield). **HRMS (EI)** Calculated for $[M+H]^+$: 501.0449. Experimental $[M+H]^+$: 501.0474. **^{1}H NMR** (399.86 MHz, $CDCl_3$) δ 7.36–7.27 (m, 10H). **^{19}F NMR** (470.14 MHz, $CDCl_3$) δ -120.19 to -120.41 (m, 1F), -135.08 to -135.27 (m, 1F), -137.64 to -137.86 (m, 2F), -149.73 to -150.08 (m, 2F), -151.47 (t, *J* = 20.8 Hz, 1F), -161.06 to -161.32 (m, 2F). **^{31}P NMR** (161.88 MHz, $CDCl_3$) δ -10.98 to -11.68 (m, 1P). **^{13}C NMR** (100.56 MHz, $CDCl_3$) δ 150.0, 145.6, 144.4, 142.1, 142.1, 141.8, 137.7, 133.1 (dd, *J* = 9.7, 2.6 Hz), 132.5 (dd, *J* = 20.3, 1.7 Hz), 129.2, 128.6 (d, *J* = 6.9 Hz) (Fluorine-bonded carbon shifts were determined by ^{13}C-^{19}F HSQC. Signals are expected to be doublets with $J^1_{C\text{-}F} > 220$ Hz).

Dicyclohexyl(perfluoro-[1,1'-biphenyl]-2-yl)phosphine (L^6). This compound was obtained 2-bromo-2',3,3',4,4',5,5',6,6'-nonafluoro-1,1'-biphenyl (0.612 g, 1.55 mmol) and Cy_2PCl (0.38 mL, 1.70 mmol). It was purified by column chromatography using *n*-hexane and recrystallized from *n*-hexane/ethanol to obtain a colorless solid (635.4 mg, 80 % yield). **HRMS (EI)** Calculated for $C_{24}H_{22}F_9P$ $[M]^+$: 512.1310. Experimental $[M]^+$: 512.1313. **^{1}H NMR** (399.86 MHz, $CDCl_3$) δ 2.26 to 2.12 (m, 2H), 1.78 to 1.60 (m, 8H), 1.45 to 1.35 (m, 2H), 1.22 to 0.90 (m, 10H). **^{19}F NMR** (376.19 MHz, $CDCl_3$) δ -124.10 to -124.32 (m, 1F), -135.06 to -135.24 (m, 1F), -137.18 to -137.41 (m, 2F), -151.32 to -151.59 (m, 2F), -152.31 (t, *J* = 20.8 Hz, 1F), -161.75 to -161.98 (m, 2F). **^{31}P NMR** (161.88 MHz, $CDCl_3$) δ 6.37 – 5.39 (m, 1P). **^{13}C NMR** (100.55 MHz, $CDCl_3$) δ 149.9, 145.5, 144.1, 141.9, 141.3, 141.3, 137.7, 34.2 (dd, *J* = 12.4, 5.1 Hz), 31.6 (d, *J* = 22.4 Hz), 30,0 (d, *J* = 7.2 Hz), 26.9 (d, *J* = 7.9 Hz), 26.8 (d, *J* = 14.3 Hz), 26.0 (d, *J* = 1.3 Hz) (Fluorine-bonded carbon shifts were determined by ^{13}C-^{19}F HSQC. Signals are expected to be doublets with $J^1_{C\text{-}F} > 220$ Hz).

Synthesis of gold(I) complexes: General procedure. [AuCl(tht)] (100 mg, 0.312 mmol) and ligand (0.312 mmol) were added to a 50 mL Schlenk flask and dissolved in 5 mL of CH_2Cl_2. The colorless solution was stirred for 30 minutes and concentrated under vacuum to about 1 mL. Then, 6 mL of *n*-hexane were added to form an interface. After two hours at 25 °C, colorless crystals were obtained. The liquid layer was filtered, and the crystals were washed with *n*-hexane (3 x 3 mL). Crystals were dried under vacuum obtaining colorless solids in all cases.

[AuCl(L^1)] (1). The general procedure was followed using [AuCl(tht)] (100.0 mg, 312 μmol) and L^1 (133.6 mg, 312 μmol). Complex **1** was obtained as a colorless solid (196.5 mg, 95 % yield). X-ray quality crystals were grown by slow diffusion of *n*-hexane in a CH_2Cl_2 solution of **1** at room temperature. **Elemental Analysis.** $C_{24}H_{14}AuClF_5P$. Calculated %: C, 43.63; H, 2.14. Experimental %: C, 43,82; H, 2.13. **^{1}H NMR** (499.73 MHz, $CDCl_3$) δ 7.68 – 7.64 (m, 1H), 7.57 – 7.52 (m, 3H), 7.50 – 7.44 (m, 8H), 7.39 (ddd, *J* = 7.8, 4.7, 1.3 Hz, 1H), 7.28 (ddd, *J* = 11.6, 7.8, 1.3 Hz, 1H). **^{19}F NMR** (470.17 MHz, $CDCl_3$) δ -137.30 to -137.53 (m, 2F), -152.09 (t, *J* = 21.1 Hz, 1F), -159.98 to -160.40 (m, 2F). **^{31}P NMR** (202.30 MHz, $CDCl_3$) δ 25.15 (s, 1P).

[AuCl(L^2)] (2). The general procedure was followed using [AuCl(tht)] (100.0 mg, 312 μmol) and L^2 (137.4 mg, 312 μmol). Complex **2** was obtained as a colorless solid (178.2 mg, 85 % yield). X-ray quality crystals were grown by slow diffusion of *n*-hexane in a CH_2Cl_2 solution of **2** at room temperature. **Elemental Analysis.** $C_{24}H_{26}AuClF_5P$. Calculated %. C, 42.84; H, 3.90. Experimental %: C, 43.07; H, 3,84. **^{1}H NMR** (499.73 MHz, $CDCl_3$) δ 7.69 – 7.63 (m, 3H), 7.35 – 7.30 (m, 1H), 2.26 – 2.16 (m, 1H), 2.07 – 1.99 (m, 2H), 1.88 – 1.81 (m, 2H), 1.81 – 1.75 (m, 2H), 1.71 – 1.64 (m, 2H), 1.45 – 1.27 (m, 7H), 1.27 – 1.14 (m, 5H). **^{19}F NMR** (470.17 MHz, $CDCl_3$) δ -139.27 to -139.40 (m, 2F), -152.42 (t, *J* = 21.2 Hz, 1F), -160.28 to -160.45 (m, 2F). **^{31}P NMR** (202.30 MHz, $CDCl_3$) δ 39.95 (s, 1P).

[AuCl(L^3)] (3). The general procedure was followed using [AuCl(tht)] (100.0 mg, 312 μmol) and L^3 (128.0 mg, 312 μmol). Complex **3** was obtained as a colorless solid (196.1 mg, 98 % yield). X-ray quality crystals were grown by slow diffusion of *n*-hexane in a CH_2Cl_2 solution of **3** at -30 °C. **Elemental Analysis.** $C_{24}H_{15}AuClF_4P$. Calculated %: C, 44.85; H, 2.35. Experimental %: C, 44.99; H, 2.40. **^{1}H NMR** (499.73 MHz, $CDCl_3$) δ 7.61 – 7.50 (m, 7H), 7.49 – 7.43 (m, 4H), 7.42 (t, *J* = 7.7 Hz, 2H), 7.02 (d, *J* = 7.6 Hz, 2H). **^{19}F NMR** (470.17 MHz, $CDCl_3$) δ -121.59 to -122.09 (m, 1F), -134.17 to -134.75 (m, 1F), -146.38 (td, *J* = 21.3, 8.6 Hz, 1F), -152.84 to -153.39 (m, 1F). **^{31}P NMR** (202.30 MHz, $CDCl_3$) δ 22.36 (s, 1P).

[AuCl(L^4)] (4). The general procedure was followed using [AuCl(tht)] (100.0 mg, 312 μmol) and L^4 (131.8 mg, 312 μmol). Complex **4** was obtained as a colorless solid (198.0 mg, 97 % yield). X-ray quality crystals were grown by slow diffusion of *n*-hexane in a CH_2Cl_2 solution of **4** at room temperature. **Elemental Analysis.** $C_{24}H_{27}AuClF_4P$. Calculated %: C, 44.02; H, 4.16. Experimental %: C, 44.19; H, 4.18. **H NMR** (499.73 MHz, $CDCl_3$) δ 7.69 – 7.64 (m, 1H), 7.55 – 7.50 (m, 2H), 7.10 – 7.06 (m, 2H), 2.54 – 2.44 (m, 2H), 2.06 – 1.97 (m, 2H), 1.87 – 1.77 (m, 4H), 1.72 – 1.65 (m, 2H), 1.60 – 1.44 (m, 4H), 1.40 – 1.21 (m, 8H). **^{19}F NMR** (470.17 MHz, $CDCl_3$) δ -124.27 to -124.47 (m, 1F), -131.70 (ddt, *J* = 23.1, 11.4, 5.1 Hz, 1F), -147.31 to -147.53 (m, 1F), -153.33 to -153.55 (m, 1F). **^{31}P NMR** (202.30 MHz, $CDCl_3$) δ 43.63 (dd, *J* = 16.7, 6.0 Hz, 1P).

[AuCl(L^5)] (5). The general procedure was followed using [AuCl(tht)] (100.0 mg, 312 μmol) and L^5 (156.1 mg, 312 μmol). Complex **5** was obtained as a colorless solid (224.1 mg, 98 % yield). X-ray quality crystals were grown by slow diffusion of *n*-hexane in a CH_2Cl_2 solution

of **5** at -30 °C. **Elemental Analysis.** $C_{24}H_{10}AuClF_9P$. Calculated %: C, 39.34; H, 1.38. Experimental %: C, 39.51; H, 1.42. **^{1}H NMR** (499.73 MHz, $CDCl_3$) δ 7.60 – 7.52 (m, 6H), 7.52 – 7.47 (m, 4H). **^{19}F NMR** (470.17 MHz, $CDCl_3$) δ -117.48 (dt, J = 21.9, 10.5 Hz, 1F), -130.21 to -130.45 (m, 1F), -137.46 to -137.72 (m, 2F), -144.03 to -144.22 (m, 1F), -147.73 to -147.91 (m, 1F), -148.03 to -148.19 (m, 1F), -158.75 to -158.96 (m, 2F). **^{31}P NMR** (202.30 MHz, $CDCl_3$) δ 22.58 (s, 1P).

[AuCl(L^6)] (6). The general procedure was followed using [AuCl(tht)] (100.0 mg, 312 μmol) and L^6 (159.9 mg, 312 μmol). Complex **6** was obtained as a colorless solid (202 mg, 87 % yield). X-ray quality crystals were grown by slow diffusion of *n*-hexane in a CH_2Cl_2 solution of **6** at -30 °C. **Elemental Analysis.** $C_{24}H_{22}AuClF_9P$. Calculated %: C, 38.70; H, 2.92. Experimental %: C, 38.90; H, 2.89. **^{1}H NMR** (499.73 MHz, $CDCl_3$) δ 2.58 – 2.48 (m, 2H), 2.09 – 2.01 (m, 2H), 1.90 – 1.77 (m, 4H), 1.73 – 1.65 (m, 2H), 1.61 – 1.49 (m, 4H), 1.44 – 1.34 (m, 4H), 1.33 – 1.19 (m, 6H). Signal at 1.61 – 1.49 integers double due to residual water in $CDCl_3$. **^{19}F NMR** (470.17 MHz, $CDCl_3$) δ -121.85 to -122.04 (m, 1F), -129.43 (ddt, J = 22.5, 10.9, 5.4 Hz, 1F), -138.26 to -138.39 (m, 2F), -145.06 to -145.21 (m, 1F), -148.29 (t, J = 21.3 Hz, 1F), -148.36 to -148.50 (m, 1F), -158.75 to -158.92 (m, 2F). **^{31}P NMR** (202.30 MHz, $CDCl_3$) δ 46.9 (d, J = 15.9 Hz, 1P).

COMPUTATIONAL DETAILS

Density Functional Theory (DFT) calculations reported in this work were carried out using the dispersion corrected hybrid functional ωB97X-D developed by Head-Gordon and Chai,[11] or B3LYP developed by Becke and Frisch,[29] with or without Grimme dispersion with the original D3 damping function,[30] implemented in the Gaussian09 program.[31] Au, P and Cl atoms were represented using the effective core potential LANL2DZ[32,33] including an f polarization function for Au (exponent 1.050)[34] and a d polarization function for P (exponent 0.387).[35] C, H and F atoms were described using the double-ζ 6-31G(d,p) basis set. Geometry optimizations were performed in vacuum and without imposing any constraint and the nature of all the stationary points was further verified through vibrational frequency analysis. Wave function files were generated from the optimized structures. QTAIM topology and Non-Covalent Interaction (NCI) analysis were carried out using wave function file (.wfn) in Multiwfn 3.7 program.[36] NCI gradient isosurfaces were depicted using VMD program.[37] NCI plots are presented at s = 0.5 and s = 0.35. Minima of sign(λ_2)ρ were extracted from grid data for s = 0.5 and s = 0.35.

SUPPORTING INFORMATION

Computational Methods and Results, X-ray Crystallography Data, NMR Spectra, SI references (36 pages).

The Supporting Information is available free of charge on the ACS Publications website.

AUTHOR INFORMATION

Corresponding Author

* P. E.: espinet@qi.uva.es

Notes

The authors declare no conflict of interest.

The authors declare no competing financial interests.

ACKNOWLEDGMENTS

The authors thank the Spanish MINECO (projects CTQ2016-80913-P and CTQ2017-89217-P), and the Junta de Castilla y León (projects VA051P17 and VA062G18). J. Ponce-de-León thanks the Spanish MINECO for an FPI scholarship (BES-2017-080726). We also thank Professor Agustí Lledós for helpful comments.

REFERENCES

[1] Martin, R.; Buchwald, S. L. Palladium-Catalyzed Suzuki-Miyaura Cross-Coupling Reactions Employing Dialkylbiaryl Phosphine Ligands. *Acc. Chem, Res*. **2008**, *41*, 1461–1473.

[2] (a) Olsen, E. P. K.; Arrechea, P. L.; Buchwald, S. L. Mechanistic Insight Leads to a Ligand Which Facilitates the Palladium-Catalyzed Formation of 2-(Hetero)Arylaminooxazoles and 4-(Hetero)Arylaminothiazoles. *Angew. Chem. Int. Ed.* **2017**, *56*, 10569–10572. (b) Leroux, F. R.; Bonnafoux, L.; Heiss, C.; Colobert, F.; Lanfranchi, D. A. A Practical Transition Metal-Free Aryl-Aryl Coupling Method: Arynes as Key Intermediates. *Adv. Synth. Catal*. **2007**, *349*, 2705–2713. (c) Mak, A. M.; Jong, H.; Robins, E. G.; Sullivan, M. B.; Lim, Y. H.; Yang, Y.; Johannes, C. W. Mechanistic Insights and Implications of Dearomative Rearrangement in Copper-Free Sonogashira Cross-Coupling Catalyzed by Pd-Cy*Phine. *Organometallics* **2016**, *35*, 1036–1045. (d) Baba, K.; Tobisu, M.; Chatani, N. Palladium-Catalyzed Direct Synthesis of Phosphole Derivatives from Triarylphosphines through Cleavage of Carbon-Hydrogen and Carbon-Phosphorus Bonds. *Angew. Chem. Int. Ed.* **2013**, *52*, 11892–11895. (e) Milne, J. E.; Buchwald, S. L. An Extremely Active Catalyst for the Negishi Cross-Coupling Reaction. *J. Am. Chem. Soc.* **2004**, *126*, 13028–13032.

[3] (a) Nieto-Oberhuber, C.; López, S.; Echavarren, A. M. Intramolecular [4 + 2] Cycloadditions of 1,3-Enynes or Arylalkynes with Alkenes with Highly Reactive Cationic Phosphine Au(I) Complexes. *J. Am. Chem. Soc.* **2005**, *127*, 6178–6179. (b) Chen, M.; Su, N.; Deng, T.; Wink, D. J.; Zhao, Y.; Driver, T. G. Controlling the Selectivity Patterns of Au-Catalyzed Cyclization−Migration Reactions. *Org. Lett.* **2019**, *21*, 1555–1558. (c) Liu, L.; Zhang, J. Gold-Catalyzed Transformations of α-Diazocarbonyl Compounds: Selectivity and Diversity. *Chem. Soc. Rev.* **2016**, *45*, 506–516. (d) Mascareñas, J. L.; Varela, I.; López, F. Allenes and Derivatives in Gold(I)- and Platinum(II)-Catalyzed Formal Cycloadditions. *Acc. Chem. Res.* **2019**, *52*, 465-479. (e) Schießl, J.; Schulmeister, J.; Doppiu, A.; Wörner, E.; Rudolph, M.; Karch, R.; Hashmi, A. S. K. An Industrial Perspective on Counter Anions in Gold Catalysis:

Underestimated with Respect to "Ligand Effects". *Adv. Synth. Catal*. **2018**, *360*, 2493-2502.

[4] (a) Li, Q.-S.; Wang, C.-Q.; Zou, R.-Y.; Xu, F.-B.; Song, H.-B.; Wan, X.-J.; Zhang, Z.-Z. Gold(I) η^2-Arene Complexes. *Inorg. Chem*. **2006**, *45*, 1888–1890. (b) Herrero-Gómez, E.; Nieto-Oberhuber, C.; López, S.; Benet-Buchholz, J.; Echavarren, A. M. Cationic η^1/η^2-Gold(I) Complexes of Simple Arenes. *Angew. Chem. Int. Ed.* **2006**, *45*, 5455–5459. (c) Partyka, D. V; Robilotto, T. J.; Zeller, M.; Hunter, A. D.; Gray, T. G. Dialkylbiarylphosphine Complexes of Gold(I) Halides. Gold−Aryl π-Interactions in the Solid State. *Organometallics* **2008**, *27*, 28–32. (d) Pérez-Galán, P.; Delpont, N.; Herrero-Gómez, E.; Maseras, F.; Echavarren, A. M. Metal-Arene Interactions in Dialkylbiarylphosphane Complexes of Copper, Silver, Gold. *Chem. Eur. J.* **2010**, *16*, 5324–5332. (e) Hashmi, A. S. K.; Bechem, B.; Loos, A.; Hamzic, M.; Rominger, F.; Rabaa, H. Gold Catalysis: Biarylphosphine Ligands as Key for the Synthesis of Dihydroisocoumarines. *Aust. J. Chem.* **2014**, *67*, 481-499. (f) Touil, M.; Bechem, B.; Hashmi, A. S. K.; Engels, B.; Omary, M. A.; Rabaâ, H. Theoretical Study of Weak CC Double Bond Coordination In Gold(I) Precursor. *Theochem*. **2010**, *957*, 21-25.

[5] Moreno-Alcántar, G.; Hess, K.; Guevara-Vela, J. M.; Rocha-Rinza, M. T.; Pendás, A. M.; Flores-Álamo, M.; Torrens H. π-Backbonding and non-covalent interactions in the JohnPhos and polyfluorothiolate complexes of gold(I). *Dalton Trans*. **2017**, *46*, 12456–12465.

[6] Jover, J.; Cirera, J. Computational assessment on the Tolman cone angles for P-ligands. *Dalton Trans.* **2019**, *48*, 15036–15048.

[7] L^1 and some Pd complexes were recently reported: Pérez-Iglesias, M.; Infante, R.; Casares, J. A.; Espinet, P. The Intriguing Behavior of an Apparently Simple Coupling Promoter Ligand, $PPh_2(p\text{-}C_6H_4\text{-}C_6F_5)$, in their Pd Complexes. *Organometallics* **2019**, *38*, 3688−3695.

[8] Barnes, N. A.; Flower, K. R.; Fyyaz, S. A.; Godfrey, S. M.; McGown, A. T.; Miles, P. J.; Pritchard, R. G.; Warren, J. E. Can the solid state structures of the dihalogen adducts R_3EX_2 (E = P, As; R = alkyl, aryl; X = Br, I) with the molecular spoke geometry be considered good mimics of the gold(I) systems $[(R_3E)AuX]$ (E = As, P; R = alkyl, aryl; X = Cl, Br, I)? *CrystEngComm* **2010**, *12*, 784–794.

[9] (a) Bondi, A. Van der Waals Volumes and Radii. *J. Phys. Chem*., **1964**, *68*, 441–451. (b) Bondi, A. van der Waals Volumes and Radii of Metals in Covalent Compounds *J. Phys. Chem.* **1966**, *70*, 3006–3007.

[10] Smith, D. G. A.; Burns, L. A.; Konrad Patkowski, K.; Sherrill, C. D. Revised Damping Parameters for the D3 Dispersion Correction to Density Functional Theory. *J. Phys. Chem. Lett.* **2016**, *7*, 2197−2203.

[11] Chai, J. Da; Head-Gordon, M. Long-Range Corrected Hybrid Density Functionals with Damped Atom-Atom Dispersion Corrections. *Phys. Chem. Chem. Phys.* **2008**, *10*, 6615–6620.

[12] This contraction obeys the strong tendency to minimize void space in condensed matter states: *Nature abhors a vacuum* (attributed to Aristotle). The effect disappears in the optimized structure of a single molecule in gas phase.

[13] Vasilyev, A. V.; Lindeman, S. V.; Kochi, J. K. Noncovalent Binding of the Halogens to Aromatic Donors. Discrete Structures of Labile Br_2 Complexes with Benzene and Toluene. *Chem. Commun.* **2001**, 909–910.

[14] Farrugia, L. J.; Evans, C; Tegel, M. Chemical Bonds without "Chemical Bonding"? A Combined Experimental and Theoretical Charge Density Study on an Iron Trimetylenemethane Complex. *J. Phys. Chem. A* **2006**, *110,* 7952–7961.

[15] Batsanov, S.S. Van der Waals Radii of Elements. *Inorg. Mater*. **2001**, *37*, 871.

[16] Alvarez, S. A cartography of the van der Waals territories. *Dalton Trans*. **2013**, 8617–8636.

[17] Atoms in Molecules: A Quantum Theory. Bader, R.F.W. Oxford University Press: Oxford, U.K., 1990.

[18] The Quantum Theory of Atoms in Molecules. Matta C. F. and Boyd R. J., eds. WILEY-VCH Verlag GmbH & Co. KGaA, Weinheim, 2007.

[19] Bohórquez, H. J.; Boyd, R. J.; Matta, C. F. Molecular Model with Quantum Mechanical Bonding Information. *J. Phys. Chem. A* **2011**, *115*, 12991–12997.

[20] The shortest Cl–C contact for L^5 is to C^4, which is apparently due to the structural influence of a particularly strong aryl-aryl interaction in this structure.

[21] Johnson, E. R.; Keinan, S.; Mori-Sánchez, P.; Contreras-García, J.; Cohen, A. J.; Yang, W. Revealing Noncovalent Interactions. *J. Am. Chem. Soc.* **2010**, *132*, 6498–6506.

[22] (a) Shahbazian, S. Why Bond Critical Points Are Not "Bond" Critical Points. *Chem. Eur. J.* **2018**, *24*, 5401–5405. (b) Foroutan–Nejad, C.; Shahbazian, S.; Marek, R. Toward a Consistent interpretation of the QTAIM: Tortuous Link between Chemical Bonds, Interactions, and Bond/Line Paths. *Chem. Eur. J.* **2014**, *20*, 10140–10152.

[23] Williams, D. B. G.; Lawton, M. Drying of Organic Solvents: Quantitative Evaluation of the Efficiency of Several Desiccants. *J. Org. Chem.* **2010**, *75*, 8351–8354.

[24] Uson, R.; Laguna, A.; Laguna, M.; Briggs, D. A.; Murray, H. H.; Fackler, J. P. (Tetrahydrothiophene)Gold(I) or Gold(III) Complexes. *Inorganic Synthesis* **1989**; *26*, 85–91.

[25] Li, Z.; Twieg, R. J. Photocyclodehydrofluorination. *Chem. Eur. J.* **2015**, *21*, 15534–15539.

[26] Oldham, P. H.; Williams, G. H.; Wilson, B. A. Homolytic Reactions of Perfluoroaromatic Compounds. Part III. Reactions of Benzoyl Peroxide with Hexafluorobenzene, Chloro-, Bromo-, and Nitro-Pentafluorobenzene, and Pentafluoropyridine. *J. Chem. Soc. B Phys. Org.* **1970**, 1346–1346.

[27] Fenton, D. E.; Massey, A. G. Perfluorophenyl Derivatives of the Elements—VI. *Tetrahedron* **1965**, *21*, 3009–3018.

[28] Keeping that temperature was crucial in order to avoid undesired products, due to formation of benzyne species by alpha-fluorine elimination at higher temperatures. Dommaschk, M.; Näther, C.; Herges, R. Synthesis of Functionalized Perfluorinated Porphyrins for Improved Spin Switching. *J. Org. Chem.* **2015**, *80*, 8496–8500.

[29] (a) Becke, A. D. Density-functional thermochemistry. III. The role of exact exchange. *J. Chem. Phys.***1993**, *98*, 5648-5652. (b) Stephens, P.J.; Devlin, F.J.; Chabalowski, C.F.; Frisch, M.J. Ab Initio Calculation of Vibrational Absorption and Circular Dichroism Spectra Using Density Functional Force Fields. *J. Phys. Chem.* **1994**, *98*, 11623-11627.

[30] Grimme, S.; Antony, J.; Ehrlich, S.; Krieg, H. A consistent and accurate ab initio parameterization of density functional dispersion correction (DFT-D) for the 94 elements H-Pu. *J. Chem. Phys*. **2010**, *132*, 154104.

[31] Gaussian 09, Revision D.01, Frisch, M. J.; Trucks, G. W.; Schlegel, H. B.; Scuseria, G. E.; Robb, M. A.; Cheeseman, J. R.; Scalmani, G.; Barone, V.; Mennucci, B.; Petersson, G. A.; Nakatsuji, H.; Caricato, M.; Li, X.; Hratchian, H. P.; Izmaylov, A. F.; Bloino, J.; Zheng, G.; Sonnenberg, J. L.; Hada, M.; Ehara, M.; Toyota, K.; Fukuda, R.; Hasegawa, J.; Ishida, M.; Nakajima, T.; Honda, Y.; Kitao, O.; Nakai, H.; Vreven, T.; Montgomery, J. A., Jr.; Peralta, J. E.; Ogliaro, F.; Bearpark, M.; Heyd, J. J.; Brothers, E.; Kudin, K. N.; Staroverov, V. N.; Kobayashi, R.; Normand, J.; Raghavachari, K.; Rendell, A.; Burant, J. C.; Iyengar, S. S.; Tomasi, J.; Cossi, M.; Rega, N.; Millam, M. J.; Klene, M.; Knox, J. E.; Cross, J. B.; Bakken, V.; Adamo, C.; Jaramillo, J.; Gomperts, R.; Stratmann, R. E.; Yazyev, O.; Austin, A. J.; Cammi, R.; Pomelli, C.; Ochterski, J. W.; Martin, R. L.; Morokuma, K.; Zakrzewski, V. G.; Voth, G. A.; Salvador, P.; Dannenberg, J. J.; Dapprich, S.; Daniels, A. D.; Farkas, Ö.; Foresman, J. B.; Ortiz, J. V.; Cioslowski, J.; Fox, D. J. Gaussian, Inc., Wallingford CT, **2009**.

[32] Hay, P. J.; Wadt, W. R. Ab Initio Effective Core Potentials for Molecular Calculations. Potentials for the Transition Metal Atoms Sc to Hg. *J. Chem. Phys*. **1985**, *82*, 270–283.
[33] Hay, P. J.; Wadt, W. R. Ab Initio Effective Core Potentials for Molecular Calculations. Potentials for K to Au Including the Outermost Core Orbitale. *J. Chem. Phys.* **1985**, *82*, 299–310.
[34] Dolg, M.; Stoll, H.; Preuss, H.; Pitzer, R. M. Relativistic and Correlation Effects for Element 105 (Hahnium, Ha): A Comparative Study of M and MO (M = Nb, Ta, Ha) Using Energy-Adjusted Ab Initio Pseudopotentials. *J. Phys. Chem.* **1993**, *97*, 5852–5859.
[35] Küchle, W.; Dolg, M.; Stoll, H.; Preuss, H. Ab Initio Pseudopotentials for Hg through Rn. *Mol. Phys.* **1991**, *74*, 1245–1263.
[36] Lu, T.; Chen, F. Multiwfn: A multifunctional wavefunction analyzer. *J. Comput. Chem.* **2012**, *33*, 580–592.
[37] Humphrey, W.; Dalke, A.; Schulten, K. VMD – Visual Molecular Dynamics. *J. Molec. Graphics* **1996**, *14*, 33–38.